Wavelength dependence of sensitivity in spectral diffuse optical imaging: effect of normalization on image reconstruction

Matthew E. Eames and Hamid Dehghani

School of Physics, Stocker Road, University of Exeter, United Kingdom,
m.e.eames@exeter.ac.uk

Abstract: Near Infrared Diffuse Optical Tomography has the potential to be used as a non-invasive imaging tool for biological tissue specifically for the diagnosis and characterization of breast cancer. Most model based reconstruction algorithms rely on calculating and inverting a large Jacobian matrix. Although this method is flexible for a wide range of complex problems, it usually results in large image artifacts from hypersensitivity around the detectors. In this work a Jacobian normalization technique is presented which takes into account the varying magnitude of different optical parameters creating a more uniform update within a spectral image reconstruction model. Using simulated data the Jacobian normalization method is used to reconstructed images of absolute chromophore and scattering parameters which are qualitatively and quantitatively as compared to conventional methods. The hypersensitivity resulting in boundary artifacts are shown to be minimized with only a small additional computational cost.

OCIS codes: (100.3190) Inverse problems; (170.3660) Light propagation in tissues; (170.4580)

References and links

1. A. P. Gibson, J. C. Hebden, and S. R. Arridge, "Recent advances in diffuse optical imaging," Phys. Med. Biol. **50**, R1-R43 (2005).
2. S. Srinivasan, B. W. Pogue, S. Jiang, H. Dehghani, C. Kogel, S. Soho, J. J. Gibson, T. D. Tosteson, S. P. Poplack, and K. D. Paulsen, "Interpreting Hemoglobin and Water Concentration, Oxygen Saturation and Scattering Measured In Vivo by Near-Infrared Breast Tomography," PNAS **100**, 12349-12354 (2003).
3. H. Dehghani, B. W. Pogue, S. P. Poplack, K. D. Paulsen, "Multiwavelength Three-Dimensional Near-Infrared Tomography of the Breast: Initial Simulation, Phantom, and Clinical Results," Appl. Opt. **42**, 135-145 (2003).
4. R. Choe, A. Corlu, K. Lee, T. Durduran, S. D. Konecky, M. Grosicka-Koptyra, S. R. Arridge, B. J. Czerniecki, D. L. Fraker, A. DeMichele, B. Chance, M. A. Rosen, and A. G. Yodh, "Diffuse optical tomography of breast cancer during neoadjuvant chemotherapy: A case study with comparison to MRI," Med. Phys. **32**, 1128-1139 (2005).
5. G. Boverman, Q. Fang, S. A. Carp, E. L. Miller, D. H. Brooks, J. Selb, R. H. Moore, D. B. Kopans, and D. A. Boas, "Spatio-temporal imaging of the hemoglobin in the compressed breast with diffuse optical tomography," Phys. Med. Biol. **52**, 3619–3641 (2007).
6. J. C. Hebden, A. Gibson, T. Austin, R. Yusof, N. Everdell, D. T. Delpy, S. R. Arridge, J. H. Meek, J. S. Wyatt, "Imaging changes in blood volume and oxygenation in the newborn infant brain using three-dimensional optical tomography," Phys. Med. Biol. **49**, 1117-1130 (2004).
7. D. A. Boas, K. Chen, D. Grebert, and M. A. Franceschini, "Improving the diffuse optical imaging spatial resolution of the cerebral hemodynamic response to brain activation in humans," Opt. Lett. **29**, 1506-1508 (2004).
8. B. W. Zeff, B. R. White, H. Dehghani, B. L. Schlaggar, and J. P. Culver, "Retinotopic mapping of adult human visual cortex with high-density diffuse optical tomography," PNAS **104**, 12169-12174 (2007).
9. M. A. Franceschini, S. Fantini, J. J. Thompson, J. P. Culver, and D. A. Boas, "Hemodynamic evoked response of the sensorimotor cortex measured non-invasively with near-infrared optical imaging," Psychophysiology **40**, 548–560 (2003).
10. H. Dehghani, B. W. Pogue, S. Jiang, B. Brooksby, and K. D. Paulsen, "Three Dimensional Optical Tomography: Resolution in Small Object Imaging," Appl. Opt. **42**, 3117-3128 (2003).

#101039 - $15.00 USD Received 2 Sep 2008; revised 14 Oct 2008; accepted 15 Oct 2008; published 17 Oct 2008

11. H. Xu, R. Springett, H. Dehghani, B. W. Pogue, K. D. Paulsen, and J. F. Dunn, "MRI coupled Broadband Near Infrared Tomography System for Small Animal Brain Studies," Appl. Opt. **44**, 2177-2188 (2005).
12. H. Xu, H. Dehghani, B. W. Pogue, R. Springett, K. D. Paulsen, and J. Dunn, "Near-infrared imaging in the small animal brain: optimization of fiber positions," J. Biomed. Opt. **8**, 102-110 (2003).
13. V. Ntziachristos, "Fluorescence Molecular Imaging," Rev. Biomed. Eng. **8**, 1-33 (2006).
14. G. Zacharakis, H. Kambara, H. Shih, J. Ripoll, J. Grimm, Y. Saeki, R. Weissleder, and V. Ntziachristos, "Volumetric tomography of fluorescent proteins through small animals in vivo," PNAS **102**, 18252-18257 (2005).
15. S. R. Arridge, "Optical tomography in medical imaging," Inverse Prob. **15**, R41-R93 (1999).
16. X. Wang, B. W. Pogue, S. Jiang, H. Dehghani, X. Song, S. Srinivasan, B. A. Brooksby, K. D. Paulsen, C. Kogel, S. P. Poplack, and W. A. Wells, "Image reconstruction of effective Mie scattering parameters of breast tissue in vivo with near-infrared tomography," J. Biomed. Opt. **11**, 041106 (2006).
17. S. Srinivasan, B. W. Pogue, B. Brooksby, S. Jiang, H. Dehghani, C. Kogel, S. P. Poplack, and K. D. Paulsen, "Near-Infrared Characterization of Breast Tumors In Vivo using Spectrally-Constrained Reconstruction," Technol. Cancer Res. Treat. **5**, 513-526 (2005).
18. A. Corlu, R. Choe, T. Durduran, K. Lee, M. Schweiger, S. R. Arridge, E. M. C. Hillman, and A. G. Yodh, "Diffuse optical tomography with spectral constraints and wavelength optimization," Appl. Opt. **44**, 2082-2093 (2005).
19. A. Li, Q. Zhang, J. P. Culver, E. L. Miller, and D. A. Boas, "Reconstructing chromosphere concentration images directly by continuous-wave diffuse optical tomography," Opt. Lett. **29**, 256-258 (2004).
20. A. Torricelli, A. Pifferi, A. Taroni, E. Giambattistelli, and R. Cubeddu, "In vivo optical characterization of human tissues from 610 to 1010 nm by time-resolved reflectance spectroscopy," Phys. Med. Biol. **46**, 2227–2237 (2001).
21. N. Shah, A. Cerussi, C. Eker, J. Espinoza, J. Butler, J. Fishkin, R. Hornung, and B. Tromberg, "Noninvasive functional optical spectroscopy of human breast tissue," PNAS **98**, 4420-4425 (2001).
22. B. J. Tromberg, N. Shah, R. Lanning, A. Cerussi, J. Espinoza, T. Pham, L. Svaasand, and J. Butler, "Non-invasive in vivo characterization of breast tumors using photon migration spectroscopy," Neoplasia (New York) **2**, 26-40 (2000).
23. M. A. Franceschini, S. Fantini, L. A. Paunescu, J. S. Maier, and E. Gratton, "Influence of a superficial layer in the quantitative spectroscopic study of strongly scattering media," Appl. Opt. **37**, 7447-7458 (1998).
24. S. R. Arridge, and W. R. B. Lionheart, "Nonuniqueness in diffusion-based optical tomography," Opt. Lett. **23**, 882-884 (1998).
25. J. C. Hebden, S. R. Arridge, and D. T. Delpy, "Optical imaging in medicine: I. Experimental techniques," Phys. Med. Biol. **42**, 825-840 (1997).
26. V. Ntziachristos, X. H. Ma, and B. Chance, "Time-correlated single photon counting imager for simultaneous magnetic resonance and near-infrared mammography," Rev. Sci. Instrum. **69**, 4221-4233 (1998).
27. M. S. Patterson, C. B., and B. C. Wilson, "Time resolved reflectance and transmittance for the non-invasive measurement of tissue optical properties," Appl. Opt. **28**, 2331-2336 (1989).
28. T. O. McBride, B. W. Pogue, S. Jiang, U. L. Osterberg, and K. D. Paulsen, "Development and Calibration of a Parallel Modulated Near-Infrared Tomography System for Hemoglobin Imaging In Vivo," Rev. Sci. Instrum. **72**, 1817-1824 (2001).
29. M. E. Eames, Wang, J., Pogue, B. W., and Dehghani, H., "Wavelength Band Optimisation in Spectral Near-Infrared Optical Tomography Improves Accuracy While Reducing Data Acquisition and Computational Burdon," J. Biomed. Opt. In Press (2008).
30. J. Wang, S. C. Davis, S. Srinivasan, S. Jiang, B. W. Pogue, and K. D. Paulsen, "Spectral tomography with diffuse near-infrared light: inclusion of broadband frequency domain spectral data," J. Biomed. Opt.**13** (2008).
31. B. Brooksby, S. Srinivasan, S. Jiang, H. Dehghani, B. W. Pogue, K. D. Paulsen, J. Weaver, C. Kogel, and S. P. Poplack, "Spectral-prior information improves Near-Infrared diffuse tomography more than spatial-prior," Opt. Lett. **30**, 1968-1970 (2005).
32. H. Dehghani, M. E. Eames, P. K. Yalavarthy, S. C. Davis, S. Srinivasan,C. M. Carpenter, B. W. Pogue, and K. D. Paulsen, "Near Infrared Optical Tomography using NIRFAST: Algorithms for Numerical Model and Image Reconstruction Algorithms," Communications in Numerical Methods in Engineering In Press (2008).
33. A. H. Hielscher, Bartel, S., "Use of penalty terms in gradient-based iterative reconstruction schemes for optical tomography," J. Biomed. Opt. **6**, 183-192 (2001).
34. M. J. Eppstein, D. J. Hawrysz, A. Godavarty, and E. M. Sevick-Muraca, "Three-dimensional, Baysian image reconstruction from sparse and noisy data sets: Near-infrared fluorescence tomography," PNAS **99**, 9619-9624 (2002).
35. H. B. Jiang, K. D. Paulsen, U. L. Osterberg, and M. S. Patterson, "Frequency-domain optical image reconstruction in turbid media: An experimental study of single-target detectability," Appl. Opt. **36**, 52-63 (1997).
36. W. Zhu, Y. Wang, Y. Yao, J. Chang, H. L. Graber, and R. L. Barbour, "Iterative total least-squares image reconstruction algorithm for optical tomography by the conjugate gradient method," J. Opt. Soc. Am. A **14**, 799-807 (1997).
37. S. Srinivasan, B. W. Pogue, S. Jiang, H. Dehghani, and K. D. Paulsen, "Spectrally Constrained Chromophore and Scattering NIR Tomography Provides Quantitative and Robust Reconstruction," Appl. Opt. **44**, 1858-1869 (2005).

#101039 - $15.00 USD Received 2 Sep 2008; revised 14 Oct 2008; accepted 15 Oct 2008; published 17 Oct 2008

38. J. R. Mourant, T. Fuselier, J. Boyer,T. M. Johnson, and I. J. Bigio, "Predictions and measurements of scattering and absorption over broad wavelength ranges in tissue phantoms," Appl. Opt. **36**, 949-957 (1997).
39. S. R. Arridge and M. Schweiger, "Photon-measurement density functions. Part2: Finite-element-method calculations," Appl. Opt. **34**, 8026-8037 (1995).
40. P. K. Yalavarthy, H. Dehghani, B. W. Pogue, and K. D. Paulsen, "Critical computational aspects of near infrared circular tomographic imaging: Analysis of measurement number, mesh resolution and reconstruction basis," Opt. Express **14**, 6113-6127 (2006).
41. M. E. Eames, B. W. Pogue, P. K. Yalavarthy, and H. Dehghani, "An efficient Jacobian reduction method for diffuse optical image reconstruction," Opt. Express **15**, 15908-15919 (2007).
42. S. Prahl, http://omlc.ogi.edu/spectra.
43. S. C. Davis, H. Dehghani, J. Wang, S. Jiang, B. W. Pogue, and K. D. Paulsen, "Image-guided diffuse optical fluorescence tomography implemented with Laplacian-type regularization," Opt. Express **15**, 4066-4082 (2007).
44. T. O. McBride, B. W. Pogue, U. L. Osterberg, and K. D. Paulsen, "Strategies for absolute calibration of near infrared tomographic tissue imaging," Oxygen Transport to Tissue XXIV, 85-99 (2003).

1. Introduction

Near Infrared (NIR) Diffuse Optical Tomography (DOT) has potential to be used as a non-invasive imaging tool for the diagnosis and characterization of breast cancer [1-5], quantifying brain function [6-9] as well as small animal imaging to study disease detection, progression and treatment [10-14]. In DOT, NIR light between the wavelengths 650 nm and 950 nm is injected into the tissue being imaged, typically using optical fibers at the external surface. The emerging fluence or *'boundary data'* is then used in a light propagation model to derive the functional parameters of hemoglobin, oxygen saturation, water content and scattering properties [3, 15, 16] typically using a spectrally constrained image reconstruction approach [17-19]. Spectroscopic transmission and/or reflectance measurements from biological tissue have also been used to demonstrate the applicability of this technique for detection and characterization of normal and diseased tissue without the need for complex image reconstruction techniques [20-23].

It has been accepted that using a continuous wave (CW) DOT system, whereby only the intensity of the NIR light travelling through tissue is measured, the problem of reconstructing optical absorption and scatter is non-unique [24]. Time-resolved systems which rely on photon counting can provide data about the time of flight of photons through the tissue [25-27]. However although these systems have historically been expensive in comparison to CW systems and are not typically used in a tomographic setting, they are becoming more popular with the advances in pulsed fiber lasers and single photon detection systems. Frequency modulated systems however, have the advantage that they are cheaper to construct than time resolved systems and measure the intensity (amplitude) and phase shift of the transmitted signal, at a given frequency (typically 100 MHz) [28], which can be thought as analogous to mean time of flight measurements from a time-resolved system.

The ability to accurately reconstruct optically dependant parameters, such as the chromophore concentrations and scattering properties, is a crucial aspect in successful clinical applications of DOT. In previous work it has been shown that the correct choice of wavelengths between 650 – 930 nm can resolve chromophores and scattering amplitude accurately with minimal cross-talk using CW data alone [18, 19, 29]. However, introducing scattering power as a variable, not only increases cross talk with other parameters but also the overall image quality may be reduced since the number of unknown parameters is increased. Previous spectral work utilizing data from the frequency domain have been based on small data sets (typically 6) dependent on the range of diodes available in the experimental system. The development of broadband systems which operate in the frequency domain can theoretically overcome the uniqueness problem when reconstructing for both absorption chromophores and scattering parameters found using CW data alone while allowing the collection of large multiple wavelength data sets which can further constrain the inverse problem [29, 30]. Although the separability of chromophores using frequency domain data is generally acceptable, the accuracy of recovering scattering properties is frequently poor and artifacts are found on the boundary for all reconstructed parameters [17, 31].

#101039 - $15.00 USD Received 2 Sep 2008; revised 14 Oct 2008; accepted 15 Oct 2008; published 17 Oct 2008

Optimization based image reconstruction in DOT utilizes the calculation and incorporation of a sensitivity (Jacobian) matrix that relates a small change in optical parameters within the imaging domain to small measurable changes in the boundary data [32-36]. However, the magnitude and range of the sensitivity of different optical properties, or indeed different chromophore and scattering properties is varied, which will be demonstrated within this paper. There has been little work in the investigation of the magnitude and range of the Jacobian and its effects on image reconstruction. In this work the Jacobian normalization method is investigated which attempts to overcome the low sensitivity seen for scattering parameters when reconstructing spectral images using a frequency modulated broadband system. A Newton-type optimization scheme is implemented where the Jacobian is calculated and inverted for non-linear image reconstruction. The magnitude and distribution of the sensitivity is shown to be dependent on the optical parameter and the number and range of wavelengths chosen for image reconstruction. The inverse of the Jacobian is then shown to be dominated by parameters with high orders of magnitude, making regularization (a parameter used to determine the smoothness of the inversion process) difficult. A Jacobian normalization technique is proposed which provides a more uniform update to the reconstructed chromophores which also removes hyper-sensitivity at the boundary and simplifies the required regularization. This method reconstructs images with higher qualitative and quantitative accuracy while removing image artifacts from the boundary.

2. Theory

The path of photons within tissue is accurately modeled by the Diffusion Approximation to the Radiative Transfer Equation when the scattering coefficient is much greater than the absorption coefficient [15]. For frequency domain data the diffusion equation has the form:

$$-\nabla\cdot\kappa(\mathbf{r})\nabla\Phi(\mathbf{r},\omega)+\mu_a(\mathbf{r})+\frac{i\omega}{c_m(\mathbf{r})}\Phi(\mathbf{r},\omega)=q_0(\mathbf{r},\omega)\ , \tag{1}$$

where $q_0(\mathbf{r},\omega)$ is an isotropic source set at one scattering distance inside the boundary, $\Phi(\mathbf{r},\omega)$ is the photon fluence rate at position **r** and modulation frequency ω (100 MHz in this work). κ is the diffusion coefficient given by

$$\kappa=1/3(\mu_a+\mu_s^{'})\,, \tag{2}$$

where μ_a and μ_s' are absorption and reduced scattering coefficients respectively. $c_m(\mathbf{r})$ is the speed of light in the medium.

The inverse problem has the aim of recovering the optical properties of the volume of interest from the finite and incomplete set of boundary measurements. Image reconstruction is carried out by reducing the difference between the measured boundary data, Φ^M, and calculated boundary data, Φ^C. This objective function is given by

$$\Omega=\min_{\mu}\left\{\sum_{i=1}^{nm}\left(\Phi_i^M-\Phi_i^C\right)^2\right\}\ , \tag{3}$$

where *nm* is the total number of measurements and μ is the optical properties which are being reconstructed (μ = [μ_a , μ_s']). Image reconstruction in DOT is an ill-posed and non-linear problem. However, the inverse problem can be linearized by minimizing equation 3 with respect to the initial optical properties and taking only the first order terms from the Taylor expansion. This gives the update equation

$$\left(\mathbf{J}^T\mathbf{J}+\alpha\mathbf{I}\right)^{-1}\mathbf{J}^T\delta\Phi=\delta\mu\ , \tag{4}$$

where $\delta\mu$ is the update to the optical properties and $\delta\Phi$ is the difference between the measured and calculated data. **J** is the Jacobian matrix given by $\delta\Phi/\delta\mu$. Since the matrix $\mathbf{J}^T\mathbf{J}$ is badly conditioned, a regularization constant, α, scaled by the maximum of the diagonal of the

#101039 - $15.00 USD Received 2 Sep 2008; revised 14 Oct 2008; accepted 15 Oct 2008; published 17 Oct 2008

Hessian ($\mathbf{J}^{\mathrm{T}}\mathbf{J}$) is added to the matrix to make it diagonally dominant and is reduced at each iteration in a modified Levenberg-Marquardt approach.

Although the forward problem is solved in terms of the absorption and reduced scattering coefficients, using a multi-spectral model, one can relate the wavelength dependence of the absorbing chromophore concentrations and scattering properties to the optical parameters. From Beer's law the absorption coefficient at a given wavelength is given by a linear sum of the contribution from each absorber [37]. This can be expressed by the relationship

$$\mu_a(\lambda_i) = \sum_{n=1}^{N} \varepsilon_n(\lambda_i) c_n , \tag{5}$$

where c_n is the chromophore concentration, ε_n is the associated molar extinction coefficient and N is the total number of chromophores. The scattering coefficient can be calculated from the empirical model based on Mie scattering theory [38] given by

$$\mu_s'(\lambda) = A\lambda^{-b} , \tag{6}$$

where A is the scattering amplitude and b is the scattering power [16]. Both the scattering power and amplitude depend on the scattering center size and number density and may reflect variations in tissue composition due to different cellular, organelle and structural sizes/densities. Incorporating spectral parameters into the update equation the Jacobian can now be expressed as

$$\mathbf{J} = \left\lfloor \mathbf{J}_{c,\lambda} \quad \mathbf{J}_{A,\lambda} \quad \mathbf{J}_{b,\lambda} \right\rfloor_{\lambda=1:i} , \tag{7}$$

where i is the total number of wavelengths and each Kernel of the Jacobian is now a function of the spectral parameters such that

$$\mathbf{J}_{c,\lambda} = \frac{\partial \Phi}{\partial c} = \frac{\partial \Phi}{\partial \mu_a}\frac{\partial \mu_a}{\partial c} , \tag{8}$$

$$\mathbf{J}_{A,\lambda} = \frac{\partial \Phi}{\partial A} = \frac{\partial \Phi}{\partial \mu_s'}\frac{\partial \mu_s'}{\partial A} , \tag{9}$$

and

$$\mathbf{J}_{b,\lambda} = \frac{\partial \Phi}{\partial b} = \frac{\partial \Phi}{\partial \mu_s'}\frac{\partial \mu_s'}{\partial b} . \tag{10}$$

For spectral image reconstruction the size and form of the Jacobian matrix is dependent on the number of data points, specifically the number of sources and detectors, the number of wavelengths used to acquire data, the number of nodes in the reconstruction and the number of parameters which are required to be reconstructed. For example, given a Jacobian for 240 amplitude and phase measurements, at 6 separate wavelengths, 5 unknown parameters (oxy (HbO_2), and deoxy hemoglobin (Hb), water fraction (H_2O), scatter amplitude (A) and power (b)) for a mesh of 1000 nodes will lead to a matrix size of 2880 × 5000.

3. Jacobian normalization

The Jacobian relates a change in optical parameter to a change in boundary data and is calculated by using the Adjoint method [39]. For a given optical parameter, μ, and measurement, Φ, the Jacobian Kernel has the form

$$\mathbf{J} = \begin{bmatrix} \frac{\delta\Phi_1}{\delta\mu_1} & \frac{\delta\Phi_1}{\delta\mu_2} & \cdots & \frac{\delta\Phi_1}{\delta\mu_{nn}} \\ \frac{\delta\Phi_2}{\delta\mu_1} & \frac{\delta\Phi_2}{\delta\mu_2} & \cdots & \frac{\delta\Phi_2}{\delta\mu_{nn}} \\ \frac{\delta\Phi_3}{\delta\mu_1} & \frac{\delta\Phi_3}{\delta\mu_2} & \cdots & \frac{\delta\Phi_3}{\delta\mu_{nn}} \\ \vdots & \vdots & \ddots & \vdots \\ \frac{\delta\Phi_{nm}}{\delta\mu_1} & \frac{\delta\Phi_{nm}}{\delta\mu_2} & \cdots & \frac{\delta\Phi_{nm}}{\delta\mu_{nn}} \end{bmatrix} , \tag{11}$$

#101039 - $15.00 USD Received 2 Sep 2008; revised 14 Oct 2008; accepted 15 Oct 2008; published 17 Oct 2008

where *nn* is the number of FEM nodes and *nm* is the total number of measurements. In previous work it has been found that due to the nature of biological tissue at NIR wavelengths being highly scattering, the sensitivity far from the plane of sources and detectors is very small [40]. Using a single wavelength reconstruction method it was found that these regions do not contribute greatly to the update equation and can therefore be removed from the reconstruction with no detriment to the recovered images [41].

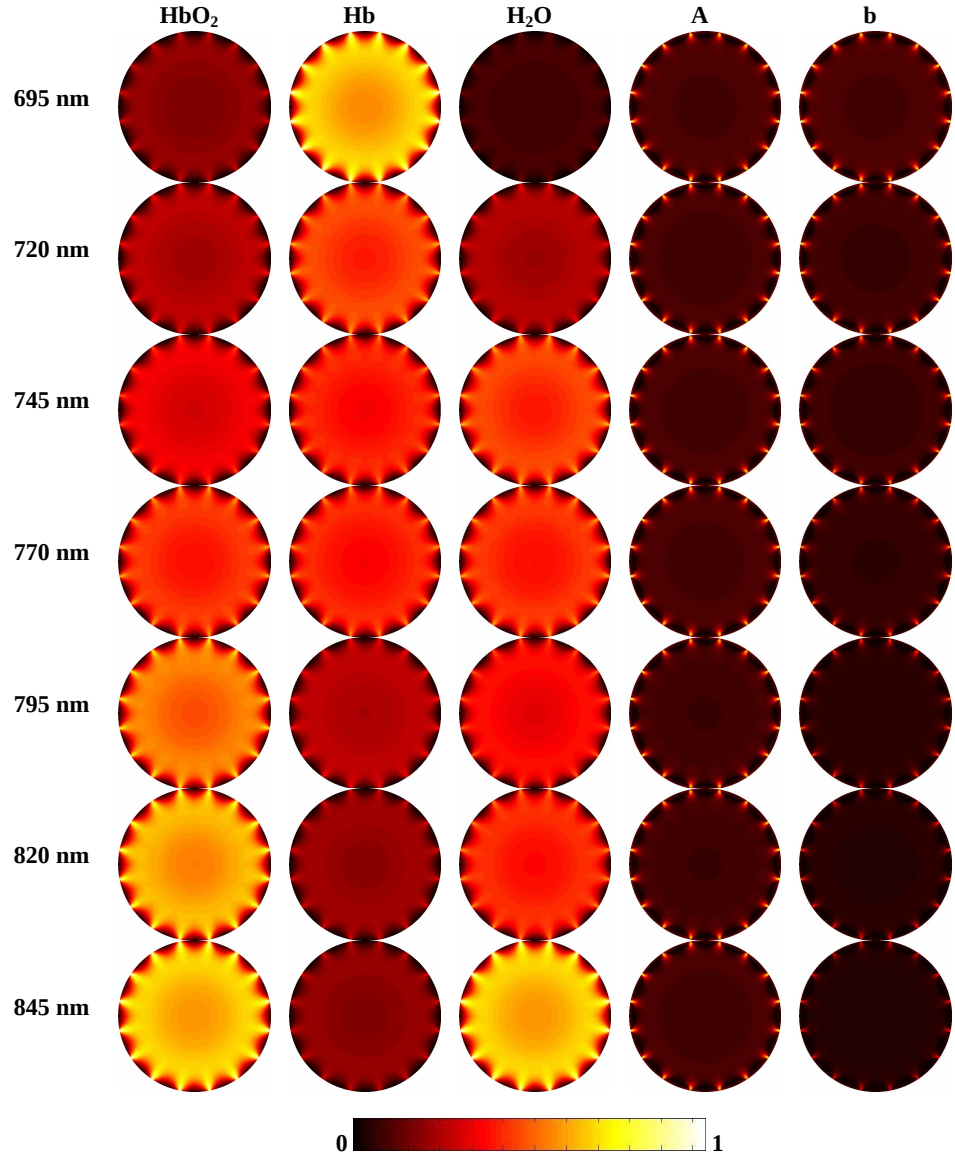

Fig. 1. Total normalised sensitivity for a set of CW data at different wavelengths. Each image represents the self normalised total sensitivity.

Using a multi-wavelength spectral model, there is a characteristic absorption and scattering property of physiologically relevant chromophores at NIR range, which is defined by the absorption and scatter spectra of tissue. In this case the total sensitivity of each chromophore will depend entirely on the range of wavelengths used; therefore it may be possible to use such spectral responses to improve image reconstruction. As an example,

#101039 - $15.00 USD Received 2 Sep 2008; revised 14 Oct 2008; accepted 15 Oct 2008; published 17 Oct 2008

consider a 2D circular model with a radius of 43 mm consisting of 16 source and detectors equidistant around the boundary with homogenous optical properties of 0.01 mM of Hb, 0.01 mM of HbO_2, 40% H_2O, and scattering amplitude and scattering power both equal to 1. Figure 1 shows the absolute normalized value of the total sensitivity at each wavelength for each chromophore and scattering property. In this case it is assumed that a measurement system has the spectral range of 695 nm to 845nm with a separation of 25 nm. The inherent spectral response for each parameter is clear. At low wavelengths the sensitivity is greatest for Hb and lowest for H_2O. At high wavelengths there is a peak in the sensitivity for HbO_2 and H_2O while there is a minimum for Hb. However the sensitivity profile is very different between scattering and absorption parameters. Although all parameters show hyper-sensitivity near the detectors, the effect is far more pronounced for the scattering parameters at all wavelengths. For absorbing chromophores the rate of change of sensitivity from the centre of the model to a detector is small. For scattering parameters, although the rate of change of sensitivity is very small from the centre of the model, the magnitude is also very much lower within a couple of scattering distances from the detectors.

Additionally, the magnitude of the sensitivity between chromophores is also dependent on the wavelengths used. In Fig. 2 the magnitude of the total sensitivity for all wavelengths is shown, where every wavelength between 695 nm and 845 nm with a 5nm separation is considered (total of 31 wavelengths). The Jacobian presented is normalized such that each Kernel has the same units, that is, it is also normalized by the mean absolute value of either the chromophore concentration or scattering properties. Although the distribution of the sensitivity of all absorption chromophores is similar, it is very different to both the distribution of scattering amplitude and scattering power and the magnitudes between all parameters is substantially different. The magnitude of the sensitivity is greatest for Hb at 120 but is approximately twice as big as HbO_2 with a magnitude of 66.6 and more than one hundred times greater than magnitude of H_2O at 0.97. Similar effects are also found for the sensitivity with phase of the measured data.

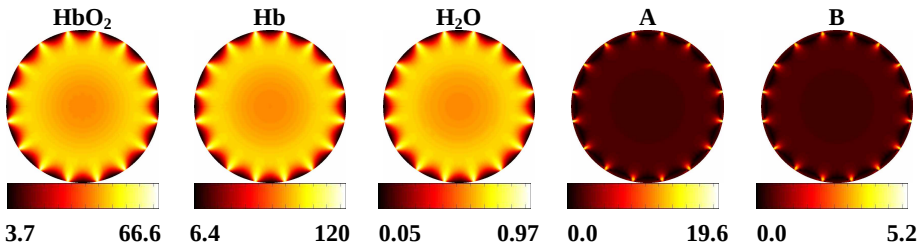

Fig. 2. Magnitude of the total sensitivity for CW data using all wavelengths between 695 nm and 845 nm with a 5nm separation (31 wavelengths).

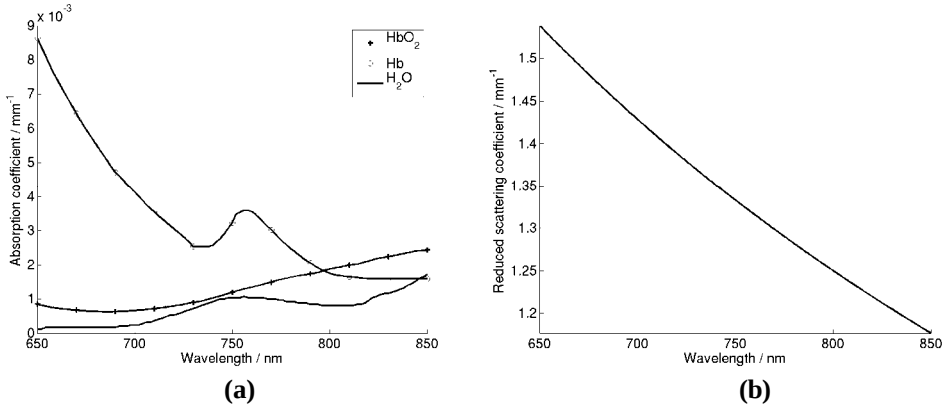

Fig. 3. (a) Absorption spectra for 0.01 mM HbO_2, 0.01 mM Hb and 40 % H_2O. (b) Empirical model fit of scattering spectra with scattering amplitude and scattering power equal to 1.

#101039 - $15.00 USD Received 2 Sep 2008; revised 14 Oct 2008; accepted 15 Oct 2008; published 17 Oct 2008

These effects of variation in spectral sensitivity distribution are a direct result of the spectral response at the wavelengths considered [42]. As shown in Fig. 3, at low wavelengths, the absorption due to Hb is much greater than that of both HbO_2 and H_2O. At around 750nm the absorption due to HbO_2 is comparable to that of Hb. At the higher end of the spectrum there is a peak in the absorption due to HbO_2 while the absorption due to H_2O and Hb is comparable but much smaller than HbO_2. It is only at much higher wavelengths (>900 nm) that the absorption due to H_2O dominates. The magnitude of the scattering parameters is largest for low wavelengths and smallest at high wavelengths.

A possible method to overcome this spectral variation of the sensitivity for different parameters is to regularize each chromophore individually within the inverse problem, Equation 4. To date, most optimization problems dealing with spectral image reconstruction has utilized a single parameter, α in Equation 4. However the choice of regularization parameter is difficult to determine and a standard method is to use an L-curve technique. But this will require a loop over each parameter for each iteration of the reconstruction to determine the optimum regularization of each parameter. This makes the reconstruction process computationally expensive.

In this proposed method, to combat the differences in the sensitivity profile, the Jacobian will be row and column normalized. This will ensure that the maximum sensitivity of each chromophore is normalized to unity as well as the sensitivity over all measurements. Pre-multiplying the Jacobian by a diagonal matrix **E** where each non-zero element is the inverse of the largest value in each column, the transformed Jacobian matrix has the form

$$\mathbf{J}_{CN} = \mathbf{E}\mathbf{J}, \tag{12}$$

where

$$E_{j,j} = \frac{1}{\max(J_{i=1:nm,\,j})} \quad . \tag{13}$$

Post-multiplying the normalized matrix by a diagonal matrix **F** where each non-zero element is the inverse of the maximum of each row of the column normalized matrix, the fully transformed Jacobian matrix has the form

$$\tilde{\mathbf{J}} = \mathbf{J}_{CN}\mathbf{F} \ , \tag{14}$$

where

$$F_{i,i} = \frac{1}{\max(J_{CN\,i,\,j=1:nn})} \ , \tag{15}$$

and the update equation is modified to

$$\mathbf{F}\left(\tilde{\mathbf{J}}^T\tilde{\mathbf{J}} + \alpha\mathbf{I}\right)^{-1}\tilde{\mathbf{J}}^T\mathbf{E}\,\delta\Phi = \delta\mu \ . \tag{16}$$

The sum of the normalized Jacobian for intensity measurements is shown in Fig. 4. In this case the magnitude of the sensitivity is similar for all parameters and has reduced the hyper sensitivity at the boundary. Since the magnitude of the sensitivity of each parameter is comparable, only one regularization parameter, α, is required.

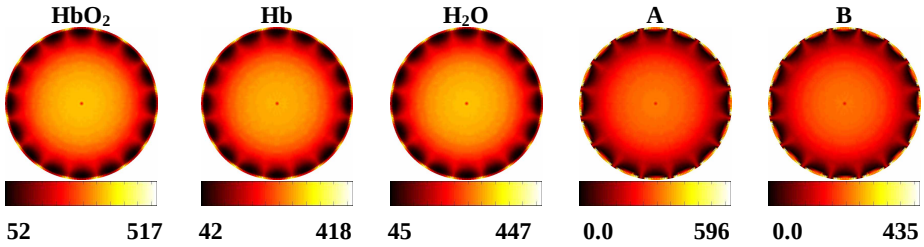

Fig. 4. Magnitude of the normalized total sensitivity for CW data using all wavelengths between 695 nm and 845 nm with a 5nm separation (31 wavelengths). Similar distributions of sensitivity are also seen with phase measurements (not shown).

#101039 - $15.00 USD Received 2 Sep 2008; revised 14 Oct 2008; accepted 15 Oct 2008; published 17 Oct 2008

4. Method and results

To compare the difference between the two reconstruction methods given by equations 4 and 16, simulations were carried out using a 2D circular model. Using a known numerical phantom has the added benefit of knowing the exact location and magnitude of the optical properties and the reconstruction methods can be compared precisely. The simulated 2D region consisted of a uniform circular mesh of radius 43mm with 1785 nodes corresponding to 3418 linear triangular elements. Sixteen optical fibers are modeled equidistant from the centre of the mesh and were used for the data collection with a modulation frequency of 100MHz giving rise 480 measurements of phase and amplitude per wavelength. The simulated data is based on a broadband system where all wavelengths between 695 nm and 845 nm with a 5nm separation are used [30]. The background has a Hb concentration of 0.01 mM, a HbO_2 concentration of 0.01 mM, H_2O content of 40%, a scattering amplitude of 0.9 and a scattering power of 0.9. Anomalies are placed uniformly around the model of radius 7.5 mm with either a Hb concentration of 0.02 mM, HbO_2 concentration of 0.02 mM, H_2O content of 80%, scattering amplitude of 1.2 and a scattering power of 1.2 as shown by Fig. 5 (left hand column). Data was simulated using the forward model and random noise is added accordingly [32].

Reconstructions using both the normalized and both non-normalized Jacobian methods are carried out using a pixel basis of 30×30 and a regularization parameter of 100. The use of pixel basis has been described elsewhere and is used to reduce the number of unknowns within the inverse problem [43]. The regularization parameter is chosen empirically as it was found to give the best results. The initial guess of physiological parameters is calculated by a global fit to the data based on the source-detector separation by use of an analytic formula for a homogeneous semi-infinite model [44]. Images were reconstructed until the projection error, the difference between the simulated and calculated data, did not improve by more than 2%.

Reconstructed images for both techniques are shown in Fig. 5 with 0% added noise and Fig. 6 for 1% added noise. It is found that the normalized method reconstructs images which are quantitatively and qualitatively more accurate than the non-normalized method. The standard reconstruction method accurately reconstructs the anomalies of Hb with a peak concentration in the region of the anomaly of 0.023 mM, HbO_2 of 0.023 mM, H_2O fraction at 90% and scattering amplitude of 1.19 with no added noise. However, it does not accurately reconstruct the scattering power anomaly with a peak value of only 0.94 with no added noise and 0.83 with 1 % added noise. Also there are image artifacts around the periphery for the standard method for all absorption chromophores which are not present when using the normalization method. With 1% added noise the reconstructed images using the standard method are qualitatively and quantitatively worse than the normalized method with more image artifacts and higher cross talk between chromophores. The standard method is particularly poor at reconstructing scattering parameters. With no added noise the normalization method reconstructs a peak in the concentration of Hb of 0.02 mM, HbO_2 of 0.019 mM, H_2O fraction of 77%, scattering amplitude of 1.26 and scattering power of 1.23.

The normalization technique reconstructs all chromophores and scattering parameters well with few image artifacts and smaller crosstalk. Similar is found for larger amounts of added noise.

It is also found that the additional computational cost of the normalization process is small as shown by Table 1. Although the computational time per iteration is larger using the normalization technique, this is compensated for by requiring fewer iterations in the reconstruction, producing images with higher quantitative and qualitative accuracy. However, the additional time is dependent on the size of the original Jacobian matrix such as, if a finer reconstruction mesh was used or more wavelengths are considered, the additional computational time would be greater.

#101039 - $15.00 USD Received 2 Sep 2008; revised 14 Oct 2008; accepted 15 Oct 2008; published 17 Oct 2008

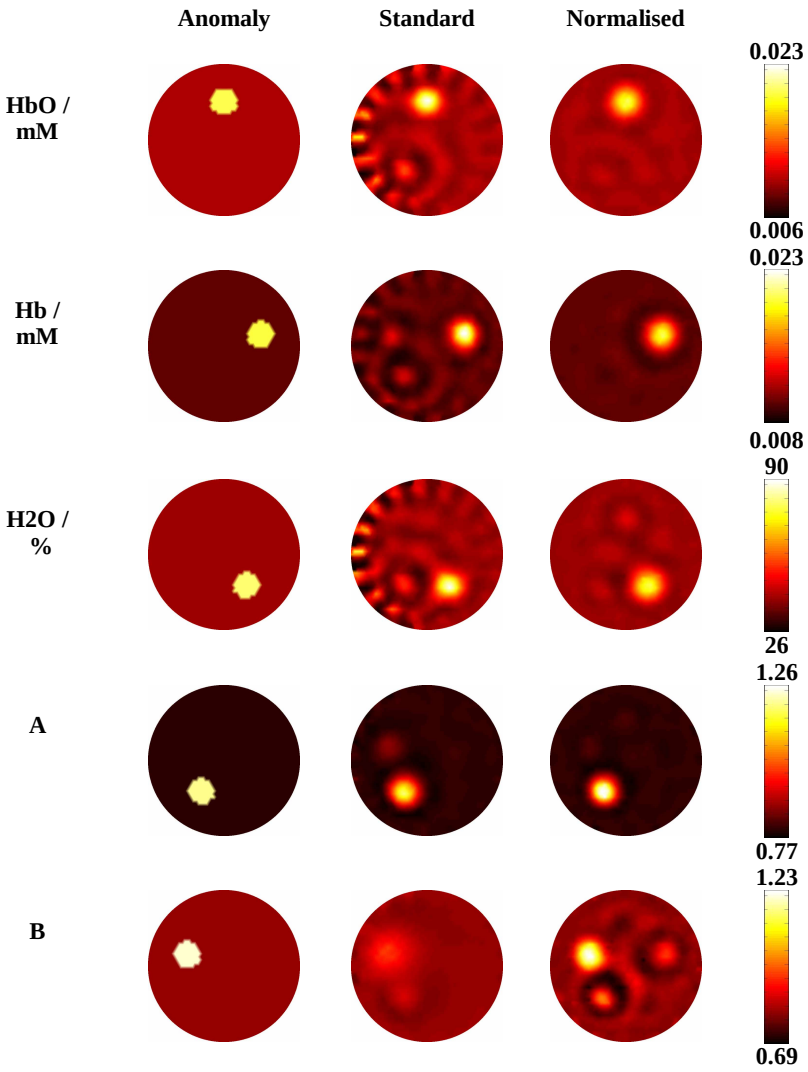

Fig. 5. Reconstructions using all wavelengths in the range 695 nm to 845 nm with separation of 5nm.

#101039 - $15.00 USD Received 2 Sep 2008; revised 14 Oct 2008; accepted 15 Oct 2008; published 17 Oct 2008

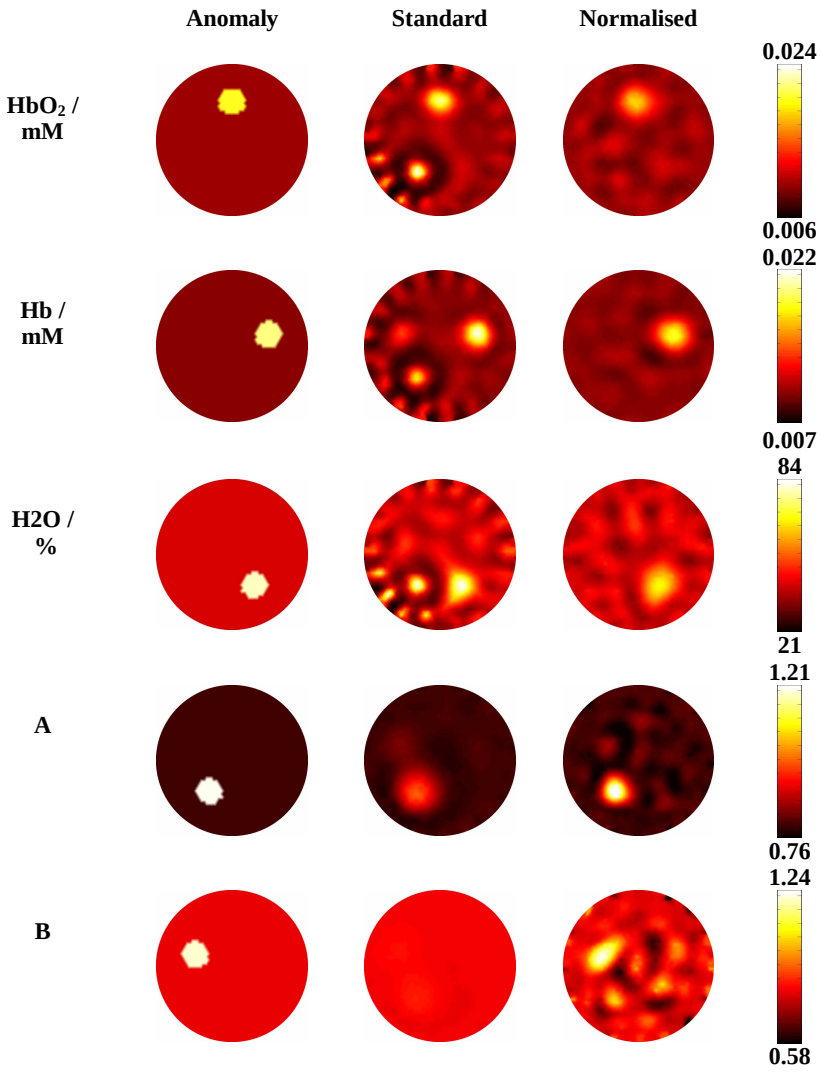

Fig. 6. Reconstructions using all wavelengths in the range 695 nm to 845 nm with a 5 nm separation and 1% added noise.

Table 1. Computational details of the two reconstruction methods.

Reconstruction method	Added noise	Number of iterations	Time per iteration
Standard	0%	27	156
	1%	21	
Normalized Jacobian	0%	19	162
	1%	17	

5. Discussions and conclusions

The sensitivity of boundary data to small changes within optical parameters within the inverse problem has been demonstrated using the calculated Jacobian. It is demonstrated that the un-normalized Jacobian for each optical parameter varies considerably in magnitude and range as compared to other parameters, specifically with the scattering parameters. A method to treat the Jacobian by row and column normalization has been presented which ensures that the

#101039 - $15.00 USD Received 2 Sep 2008; revised 14 Oct 2008; accepted 15 Oct 2008; published 17 Oct 2008

sensitivity of each optical parameter to be reconstructed using multi-wavelength is of the same order of magnitude. Using this method, the regularization used within Newton-type optimization allows for comparable smoothing across all parameters within the image reconstruction, without having bias with respect to magnitude or range of the sensitivity.

Simulated data using a simple 2D model was used as a proof of concept using 31 wavelengths in the range of 695 nm to 845 nm with both amplitude and phase data. It is shown that row and column normalizing the Jacobian matrix removes image artifacts by removing hypersensitivity at the boundary. For example, Fig. 2 demonstrates that the scattering parameters are dominated by hypersensitivity at the boundary and also the magnitude between all 5 reconstructed parameters varies greatly with magnitude of the sensitivity of H_2O being much smaller than the other parameters. Although the scattering sensitivity is still largest on the boundary, the relative sensitivity is much greater in the centre and the magnitude of all parameters is comparable. It is shown that this method reduces image artifacts as well as improved reconstructed anomalies with 1% added noise as shown by Fig. 6. Although the standard method was able to accurately reconstruct most anomalies, it was unable to reconstruct the scattering power anomaly with a peak value of 0.94 as compared to 1.26 and using the normalization method with no added noise. The additional computational cost of the normalization technique is also found to be small in comparison to the standard method.

Acknowledgments

This work has been sponsored by the Engineering and Physical Sciences Research Council, UK.

#101039 - $15.00 USD Received 2 Sep 2008; revised 14 Oct 2008; accepted 15 Oct 2008; published 17 Oct 2008